A New Temperature-Tolerant RF MEMS Switch Structure Design and Fabrication for Ka-Band Applications

Kaan Demirel, Erdem Yazgan, Şimşek Demir, *Member, IEEE*, and Tayfun Akın

***Abstract*— In this paper, the design and fabrication of a new radio frequency (RF) microelectromechanical system (MEMS) switch structure is presented. This RF MEMS switch is developed to get the minimum permanent deformation on the micro-bridge after 200 °C thermal treatment. The residual stress-based buckling on the MEMS bridge is simulated for 5–40-MPa/μm stress gradient ($\Delta\sigma$) with 5-MPa/μm steps. The temperature-dependent extension and deformation on the MEMS bridge are modeled up to 270 °C. The temperature-dependent permanent deformation on the MEMS bridge is reduced by optimizing the dimensions of the bridge. The electromechanical and electromagnetic simulations are carried out to find the actuation voltage and the RF performance at Ka-band. The actuation voltage is measured as 22 and 25 V before and after 200 °C thermal treatment for 2-μm air gap (g_0). The RF performance of the switch is measured before and after 200 °C thermal treatment to observe the temperature effect on the MEMS bridge. The persistent insertion loss (<0.35 dB) and the isolation (<−20 dB at 28–40 GHz) are measured before and after thermal treatment. The RF MEMS switch is fabricated on quartz wafer using an in-house surface micromachining process with an amorphous silicon sacrificial layer structure. [2015-0134]**

***Index Terms*— Amorphous silicon (a-Si), buckling, RF microelectromechanical systems (RF MEMS), thermal treatment, sacrificial layer, stress, temperature.**

I. Introduction

RF MEMS switches are promising candidates as components for communication system due to their low loss and high isolation properties at high RF frequencies [1]–[3]. One of the research issues on the RF MEMS switches is the temperature dependent buckling and permanent deformation on the mechanical parts [4], [5]. Especially, MEMS packaging temperature can cause the micro bridge to deform [6], [7]. This deformation affects the RF and electromechanical performance of the switch [8], [9]. An RF MEMS shunt switch has a mechanically movable micro bridge on the t-line to short the signal line to the ground when the switch is actuated. Generally, this MEMS bridge consists of a very thin single metal layer with respect to its length. This MEMS bridge has a high aspect ratio and can be buckled or permanently deformed under high temperature due to thermal expansion. The bridge buckling or permanent deformation is an undesired effect since the RF performance of the shunt switch depends on the air gap (bridge height). The temperature dependent buckling on the MEMS bridge can be reduced by using different bridge materials and well-designed bridge geometries [10]–[14]. In these works, the switch performance after high temperature (≥200 °C) treatment did not investigate. Therefore, the temperature for switch failure can not be predicted. In this work, the switch failure temperature is investigated, as well. On the other hand, the fabricated switch shows relatively low pull down voltage (<25 V).

Fixed-fixed beam type MEMS bridge structures obstruct the thermal expansion based lateral movement of the bridge. Therefore, the thermal expansion leads to out of plane deflection in this structure [15]. Moreover, the compressive effects of the temperature on the bridge leads to permanent deformation on the MEMS bridge.

In this study, the MEMS bridge geometry was designed to reduce the thermal expansion based out of plane deflection by allowing the bridge movement in lateral direction. This movement of the bridge reduces the stress level on the bridge structure and prevents the permanent deformation of the MEMS bridge. Therefore, the bridge shows the lateral movement at high temperature and returns to its original position when the temperature is restored. Based on the requirements (200 °C) of our in-house MEMS packaging process, MIMOSA, temperature dependent buckling on the MEMS bridge was modeled up to 270 °C to observe the device failure. The fabrication based residual stress and stress gradient are defined on the MEMS bridge to find the buckling values on the MEMS bridge at room temperature.

The actuation voltage of the RF MEMS switch was estimated by modeling electrostatic forces on the MEMS bridge due to potential difference between bridge and actuation electrode. The actuation voltages were estimated as <30V for 1.5 and 2 μm bridge height.

Manuscript received May 18, 2015; revised September 18, 2015; accepted September 18, 2015. This work was supported by the Scientific and Technological Research Council of Turkey under Grant 109A008. Subject Editor J.-B. Yoon.

K. Demirel is with the Department of Nanotechnology and Nanomedicine, Hacettepe University, Ankara 06800, Turkey, and also with the Department of Electrical and Electronics Engineering, Middle East Technical University, Ankara 06800, Turkey (e-mail: kdemirel@mems.metu.edu.tr).

E. Yazgan was with the Department of Nanotechnology and Nanomedicine, Hacettepe University, Ankara 06800, Turkey. She is now with the Department of Electrical and Electronics Engineering, TED University, Ankara 06420, Turkey (e-mail: erdem.yazgan@tedu.edu.tr).

Ş. Demir and T. Akın are with the Middle East Technical University–Micro-Electro-Mechanical Systems Research and Applications Center, Department of Electrical and Electronics Engineering, Middle East Technical University, Ankara 06800, Turkey (e-mail: simsek@metu.edu.tr; tayfuna@metu.edu.tr).

Color versions of one or more of the figures in this paper are available online at http://ieeexplore.ieee.org.

Digital Object Identifier 10.1109/JMEMS.2015.2485659

RF design of the switch was carried out to get low loss (<0.35 dB) in upstate and better than 20 dB isolation in downstate at Ka-band for radar applications. The designed MEMS bridge has four mechanical support areas (anchors) which are placed on the ground and on the wafer to obtain desired mechanical and RF performance.

This RF MEMS switch was fabricated on quartz wafer and the fabrication process was developed at the Middle East Technical University-MEMS Research and Application Center (METU-MEMS). The amorphous silicon (a-Si) layer was used as a sacrificial layer. The a-Si is a good candidate as a sacrificial layer for suspended MEMS devices due to its coating and etch process advantages with respect to polymer sacrificial layers. A thin Si_xN_y dielectric layer was coated on the signal line to form a capacitance between signal line and ground in the downstate position of the bridge. The MEMS bridge structural material was selected as 2 μm Au layer.

RF MEMS switch actuation voltage and RF measurements were taken before and after 200 °C thermal treatment to observe the temperature effect on the MEMS bridge. The thermal treatment was applied in the oven for 30 min. Electromechanical and RF performances are compared before and after this thermal treatment.

II. RF MEMS Switch Design

The compressive stress on the fixed-fixed beam leads to buckling of the beam structure and device failure. This stress, known as the critical stress, is given for a fixed-fixed beam by (1) [16]. The residual stress can be tensile or compressive but in general, the beam structures are fabricated with residual tensile stress to avoid the beam buckling. Beside this, the spring constant of the beam increases with increasing tensile stress and leads to higher pull down voltage. On the other hand, initial tensile stress of the beam reduces with increasing temperature. Moreover, at higher temperatures the beam stress becomes compressive and leads to buckling of the beam and device failure. Total beam stress at temperature T is given by (2), with σ_{res} is initial beam stress at temperature T_o, E is Young's modulus of the beam, α_b and α_s are thermal expansion coefficient of beam and substrate, respectively.

$$\sigma_{cr} = \frac{Et^2\pi^2}{3l^2(1-\nu)} \quad (1)$$

$$\sigma_t(T) = \sigma_{res} + (\alpha_b - \alpha_s)E(T - T_o) \quad (2)$$

Our typical fixed-fixed beam RF MEMS switch with 180 μm length (l), 80 μm width (w) and 1.2 μm thickness (t) has 18 MPa calculated critical compressive stress, for E = 70 GPa and ν = 0.44. This critical stress value was calculated by using (1). When the stress exceeds this compressive stress value, the bridge deflects in z-direction (out of plane deflection) and effects the RF and electromechanical performance of the switch. To observe the deflection and maximum stresses on the bridge the simulations were carried out for $\sigma_x = \sigma_y = 0, 10, 20, 30, 40, 50$ MPa, in-plane biaxial tensile stress. As it can be seen from Figure 1 the tensile stress on the beam reduces with increasing temperature and becomes compressive at 49 °C for 50 MPa stressed structure. Then, the

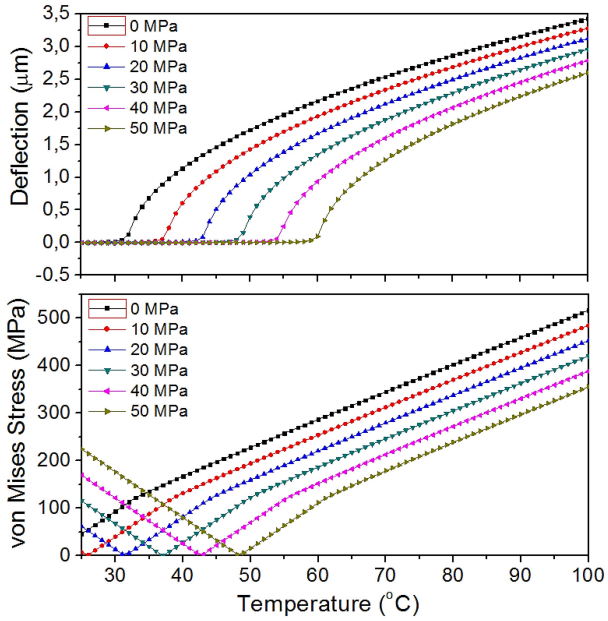

Fig. 1. Beam structure deflection and maximum von Mises stress levels on the bending region with temperature (l = 180 μm, w = 80 μm, t = 1.2μm).

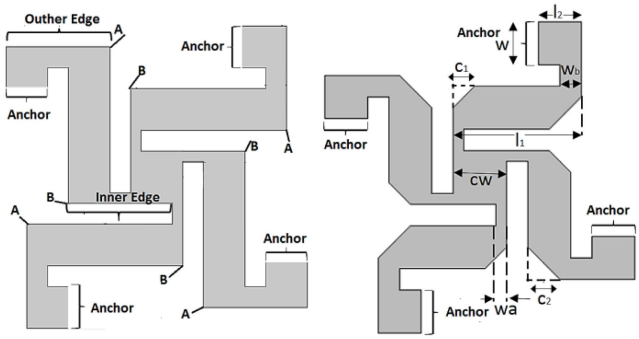

Fig. 2. (a) Un-chamfered MEMS bridge edges and points (A and B), (b) chamfered MEMS bridge structure illustration, (c) layered MEMS bridge model to build up a stress gradient on the MEMS bridge.

beam starts to buckle at 60 °C due to temperature dependent compressive stress. On the other hand, for $\sigma_x = \sigma_y = 0$ MPa the beam starts to buckle at lower temperature (< 35 °C). It can be seen the beam with high tensile stress is more robust to the temperature depended buckling, but this tensile stress leads to increase the pull in voltage of the switch.

The MEMS packaging process requires high temperatures (≥200 °C). Due to our in-house packaging temperature is 190-200 °C, a folded leg rotatable bridge structure was designed to avoid permanent deformation of the bridge at this temperature range.

First, the MEMS bridge was designed with four anchors and sharp corners on the mechanical legs (Figure 2a) and then the

TABLE I
T2 MEMS BRIDGE DIMENSIONS

Label	Value (μm)
l_1	120
l_2	40
c_1	20
c_2	30
w	40
wa	10
wb	20
cw	50

edges were chamfered to reduce the buckling at these points (labeled as A and B in Figure 2b). The un-chamfered and the chamfered designs were named as T1 and T2, respectively. Figure 2b shows the chamfered MEMS bridge geometry and the dimension labels. The corners A and B (Figure 2a) were cut 30 μm and 20 μm through edge, respectively. The dimension parameters of the T2 MEMS bridge are given in TABLE I.

During the switch design, mechanical legs of the RF MEMS switch were extended and folded to get enough thermal expansion tolerance and to get low actuation voltage. The mechanical leg dimensions of l_1 and l_2 are selected as 120 μm and 40 μm. Beside this consideration, the anchor points of the structure are placed at appropriate region for RF design of the CPW and the MEMS bridge structures.

The residual and thermal stresses effects on the MEMS bridge buckling are modeled by using COMSOL Multiphysics Modeling Software. In order to estimate the buckling on the MEMS bridge, the fabrication based residual stresses were modeled as a vertical stress gradient across the bridge thickness. To do this, the MEMS bridge are divided into two layers with equal thickness ($t_1 = t_2, t = t_1 + t_2$) and different stress values (σ_1, σ_2) and calculated by using (3) and (4) [12]. Figure 2c shows the layered MEMS bridge model to introduce the stress gradient across the MEMS bridge. The bridge buckling values were modeled for the stress gradients ($\Delta\sigma$) 5-40 MPa/μm with 5 MPa/μm step. The intrinsic stress (residual stress) of the layer 1 is assumed more tensile than that of the layer 2 and taken as $\sigma_1 > \sigma_2$.

$$\Delta\sigma = (\sigma_1 - \sigma_2)/t \quad (3)$$

$$\sigma_{avg} = (\sigma_1 t_1 + \sigma_2 t_2)/t \quad (4)$$

The $-$z direction buckling values on the inner and outer edges change with the stress gradient. On the other hand, the maximum buckling values depend on the edge geometry of the MEMS bridge. The outer edge (point a) maximum buckling values of the T1 and T2 MEMS bridges for $\Delta\sigma = 5$ MPa/μm, are 0.11 μm and 0.06 μm, respectively. The inner edge (point b) maximum buckling value of the T1 and T2 MEMS bridges for $\Delta\sigma = 5$ MPa/μm, are 0.1 μm and 0.08 μm, respectively (Figure 3 (a,b)). As it can be seen, the outer and inner edge buckling values were decreased by 45% and 20%, respectively, by cutting the A and B corners. The increased deflection with the $\Delta\sigma$ value is expected result, as well. The inner edge (point b) deflections of the T1 and T2 MEMS bridges are 0.6 μm and 0.41 μm for $\Delta\sigma = 40$ MPa/μm. As a result, the deflection values of the inner and outer edges of the cut edge T2 design are less than that of the T1 design for all $\Delta\sigma$ values. The inner (point b) and outer edge (point a) maximum deflection values for both designs are given in TABLE II and Figure 3 (c) shows the deflections at a,b,c and d points for each $\Delta\sigma$ value.

TABLE II
T1 AND T2 MEMS BRIDGE DEFLECTION VALUES ON INNER AND OUTER POINTS FOR DIFFERENT STRESS GRADIENTS

Δσ (MPa/μm)	T1 Deflection (μm)		T2 Deflection (μm)		T2/T1 (%)	
	Outer	Inner	Outer	Inner	Outer	Inner
5	0.11	0.1	0.06	0.08	55	80
10	0.23	0.17	0.13	0.13	56	76
15	0.36	0.25	0.21	0.18	58	72
20	0.48	0.32	0.29	0.22	60	69
25	0.61	0.39	0.37	0.27	61	69
30	0.74	0.46	0.44	0.32	60	70
35	0.86	0.53	0.52	0.36	61	68
40	1	0.6	0.6	0.41	60	68

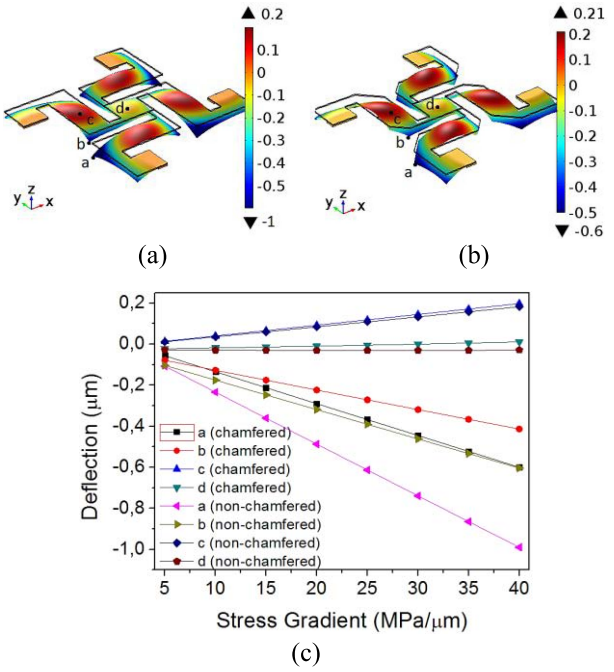

Fig. 3. (a,b) T1 (non-chamfered) and T2 (chamfered) MEMS bridge deflections for $\Delta\sigma = 40$ MPa/μm, (c) the deflection values at labeled points on T1 and T2 MEMS bridges for $\Delta\sigma = 5$-40 MPa/μm (with 5 MPa/μm step).

Our in-house sputtered 2-μm-thick gold layer has an average in-plane stress of 20 MPa and a vertical stress gradient of $\Delta\sigma \leq 10$MPa/μm (typically 5 MPa/μm).

As it can be seen, the T2 design is more acceptable than the T1 design in terms of residual stress dependent buckling tendency. Therefore, the models are carried out only for T2 MEMS bridge design after this point.

The temperature effects and the buckling values on the T2 MEMS bridges were investigated for compressive and tensile in-plane stresses. The maximum deflections on the middle part of the bridge are 0.14 μm and 0.21 μm for 50 MPa tensile and compressive stresses, respectively (Figure 4(a,b)).

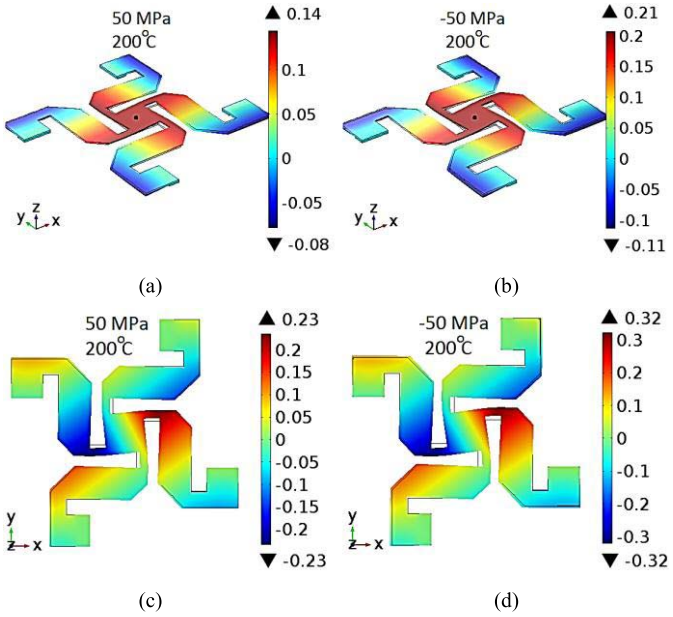

Fig. 4. The MEMS bridge deflection model for T2 design for 50 MPa tensile and compressive stresses at 200 °C. (a,b) out of plane deflection, (c,d) in-plane rotational movement model ($\sigma_{\text{avg}} = -50$, 50 MPa, $\Delta\sigma = 0$ MPa/μm).

The MEMS bridges axial rotation behavior at the 200 °C is another important design issue for these MEMS bridges. Figure 4(c,d) show the axial rotational behaviors of the MEMS bridge for tensile and compressive stresses at 200 °C. As it can be seen, the bridge structure shows the rotational movement due to the expansion of the MEMS bridge material (Au) at 200 °C. This movement decreases the deflection of the MEMS bridge parts in z direction. Especially, the MEMS bridge middle part deflection in the +z direction is reduced with this rotational movement at high temperatures. The extension in the y direction is 0.23 μm and 0.32 μm for 50 MPa tensile and compressive stresses, respectively (Figure 4(c,d)).

The stress on the MEMS bridge changes from tensile to compressive with increasing temperature. Because of that, the bridge, which has compressive in-plane stress, buckles much more than that of the tensile stressed bridge structures.

Figure 5 shows the middle part deflection of the MEMS bridge under tensile and compressive stresses for different temperature. There is no significant deflection on the middle part of the MEMS bridge for 50 °C and increases gradually with increasing temperature. For $\sigma_x = \sigma_y = -50$ MPa biaxial in-plane stress, the maximum deflection on the middle part is 0.32 μm and decreases to 0.23 μm with changing biaxial in-plane stress of the structure from compressive to tensile at 270 °C. The deflection on the middle part of the MEMS bridge at our in-house packaging temperature (200°C) is found as 0.2 μm for $\sigma_x = \sigma_y = -50$ MPa and decreases to 0.14 μm for $\sigma_x = \sigma_y = 50$ MPa.

Another important parameter for this design is "*wa*" dimension (Figure 2(b)). The temperature dependent buckling of inner and outer parts depend on the dimension of the *wa*. The rotational movement of the MEMS bridge and the stress level on inner and outer corners due to temperature depends on this dimension, as well.

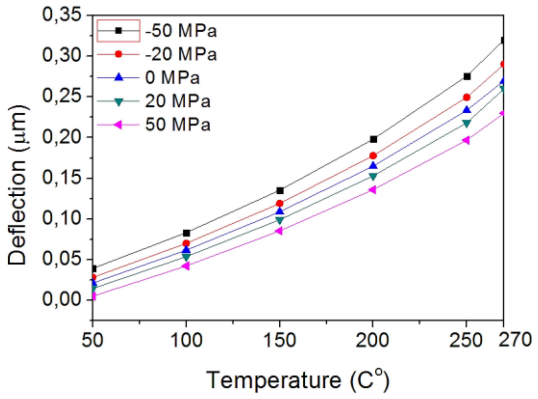

Fig. 5. MEMS bridge middle point deflection for 50, 100, 150, 200, 250, 270 °C and $\sigma_{\text{avg}} = 50, 20, 0, -20, -50$ MPa.

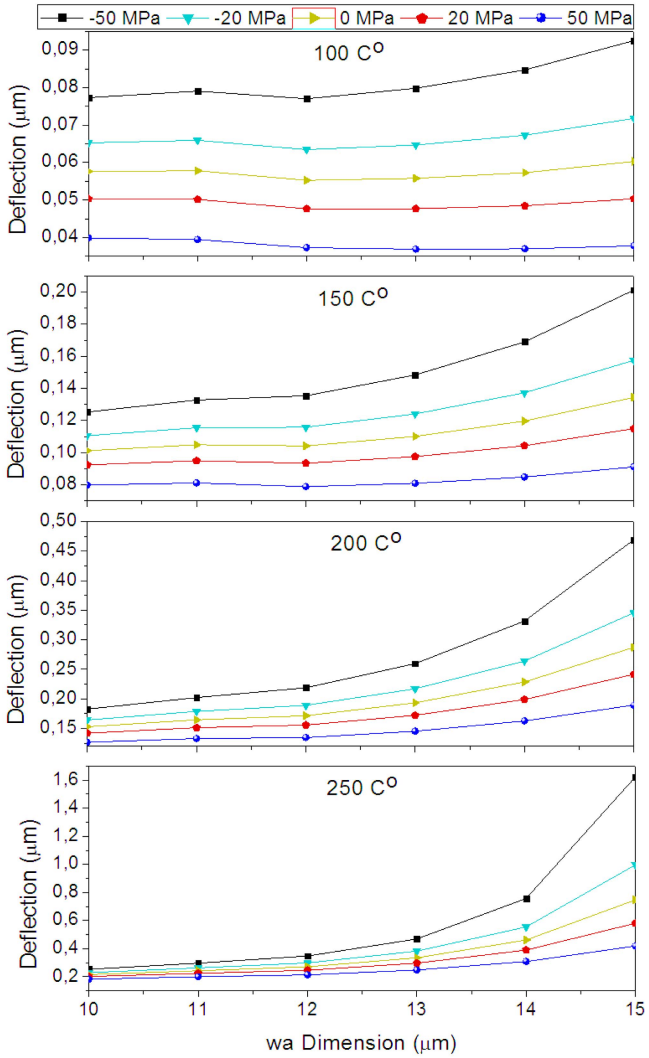

Fig. 6. The *wa* dimension effects on the MEMS bridge deflection for 100, 150, 200, 250 °C. The maximum deflection on the MEMS bridge middle point increase with increasing *wa* dimension. The deflection dependency on the *wa* dimension is not linear and increase sharply after $wa = 13$ μm.

Figure 6 shows the *wa* dimensions and the maximum deflections on the inner and outer parts of the MEMS bridge for 100-250 °C temperature range. Maximum deflection

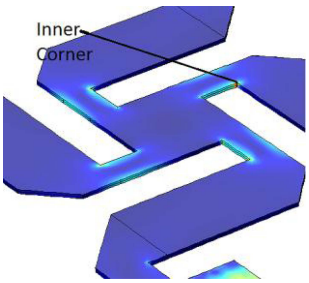

Fig. 7. The inner corner of the MEMS bridge structure. The temperature dependent rotational movement cause the stress on this corner. The stress levels on these corners is depend on the *wa* dimension.

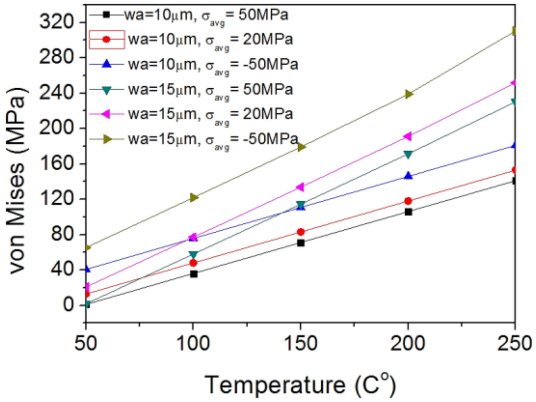

Fig. 8. The von Mises stress at the inner corners at 50, 100, 150, 200, 250 °C for $wa = 10, 15$ μm and $\sigma_{avg} = -50, 20, 50$ MPa in-plane stresses. The stress level on the corner increases with increasing *wa*.

on the middle part of the bridge increases sharply after $wa = 13$ μm. At 200 °C (for $\sigma_x = \sigma_y = -50$ MPa) the deflection decreases from 0.47 μm to 0.18 μm for $wa = 15$ and 10 μm, respectively. For 250 °C (for $\sigma_x = \sigma_y = -50$ MPa in-plane stresses) the deflection decreases from 1.62 μm to 0.25 μm for $wa = 15$ and 10 μm, respectively. Therefore, the deflection is decreased with 62 % and 85 % for 200 °C and 250 °C, respectively for −50 MPa. This behavior attributed to rotational movement tendency of the MEMS bridge with decreased *wa* dimension.

The *wa* dimension effect on the stress level inner corner is another important issue for permanent deformation of MEMS bridge. Figure 7 shows the inner corner on the MEMS bridge. The MEMS bridge rotational movement with temperature cause increasing the stress level on these corners. This stress level dependency on *wa* dimension are investigated for 50-250 °C temperature range via von Mises stress at these corners. For $wa = 15$ μm, the inner corner stress level at 200 °C is 239 MPa and 171 MPa for −50 MPa and 50 MPa in-plane stress, respectively. For $wa = 10$ μm, the inner corner stress level is reduced to 146 MPa for −50 MPa and 106 MPa for 50 MPa at 200 °C. Figure 8 shows the von Mises stresses on this corner for 50-250 °C temperature range and 50, 20 and −50 MPa in-plane stresses.

The actuation voltage was estimated by using COMSOL MEMS module. Figure 9 shows the MEMS bridge and actuation electrode. The MEMS bridge was selected as 2 μm Au. The dielectric layer was selected as 0.3 μm (t_d) Si_xN_y with the

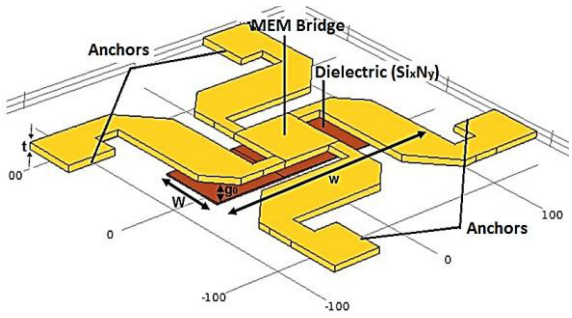

Fig. 9. The MEMS bridge and actuation electrode of the RF MEMS switch. The pull down electrode is named as dielectric (Si_xN_y).

TABLE III
MEMS BRIDGE DIMENSIONS

Symbol	Quantity	Value (μm)
W	actuation electrode width	50
w	MEMS bridge length	170
g_0	bridge height	1.5-2
t	MEMS bridge thickness	2
t_d	dielectric thickness	0.3

TABLE IV
ACTUATION VOLTAGES

t_d (μm)	g_0 (μm)	V_{ps} (V)	V_p (V)	V_o (V)	V_{pt} (V)	V_{ot} (V)
0.3	2	23	22	6.5	25	10
0.3	1.5	15.7	-	-	-	-

dielectric constant of 7. The actuation voltage was estimated for 1.5 and 2 μm air gap (g_0) between the MEMS bridge and pull down electrode. TABLE III shows the MEMS bridge dimensions.

TABLE IV shows the gap, pull down and pull out voltage values. The estimated actuation voltage for 2 μm and 1.5 μm air gap are 23 V and 15.7 V (V_{ps}), respectively. The zipping effect was neglected during the simulation.

The CV measurements were carried out to find the pull down, pull out voltages and capacitance level in down state. Figure 10 shows that the bridge shows a zipping effect before fully actuated. First, the bridge middle part is pulled down (point P_{i1} in CV graph) and then the bridge fully actuated (point P_{i2} in CV graph). RF MEMS switch actuation voltage (V_p, point P_{i2}) and fully pull out voltage (V_o, point P_o) were found as 22 V and 6.5 V before heat treatment. The capacitance level was measured as 0.6 pF in down state position. After 200 °C heat treatment the actuation voltage (V_{pt}, point P_{i2}) and fully pull out voltage (V_{ot}, point P_o) were found as 25 V and 10 V. No significant degredation was observed on RF performance of the switch after thermal treatment.

The RF MEMS switch was designed for high isolation and low loss at Ka-band. The coplanar waveguide (CPW) structure

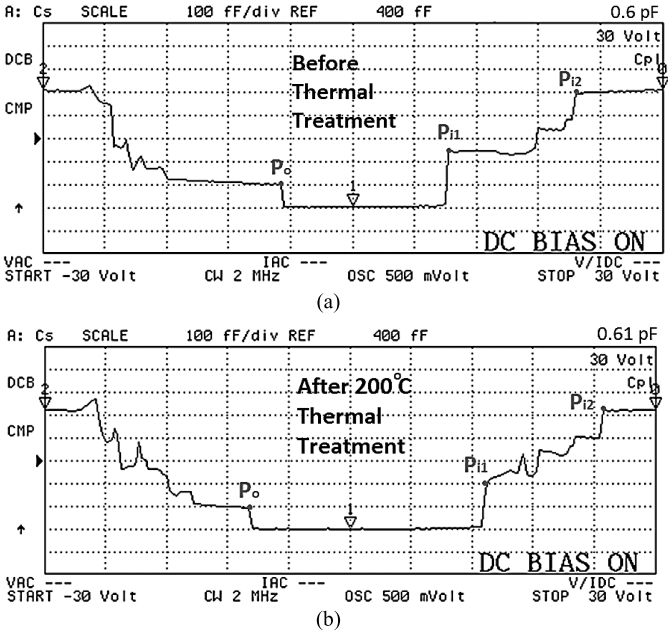

Fig. 10. RF MEMS switch CV curves a) before heat treatment, b) after 200 °C heat treatment.

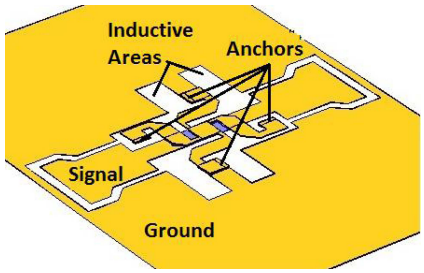

Fig. 11. The RF MEMS structure and anchor areas.

material was selected as 1 μm Au. The simulations were carried out for 1.5 and 2 μm air gap. Figure 11 shows the RF MEMS switch structure with inductive tuning areas. The MEMS bridge has four anchors. Two of them is electrically connected to the ground and the others to the quartz substrate for mechanical support. This allows easier inductive tuning on the device. The inductive tuning allows getting high isolation at Ka-band. In the next section measurement results are given following the fabrication details.

III. Fabrication and Measurements

The RF MEMS switch was fabricated on quartz wafer. The CPW structure was fabricated by using 1 μm sputtered Au layer and a 20-nm-thick Ti layer was used as adhesion layer between the Au and quartz. The dielectric layer was selected as 0.3 μm PECVD Si_xN_y layer to make a capacitance between ground and signal line in downstate position. A 2-μm-thick amorphous silicon (a-Si) layer was used as a sacrificial layer to define the air gap. The a-Si layer was deposited by using PECVD. The MEMS bridge anchor areas was defined lithographically and a-Si is etched at these areas by using DRIE system.

The structural layer (bridge layer) was coated after anchor opening process. Then the bridge structure and electroplating seed layer were formed by patterning this Au layer. The structural layer was fabricated as 2 μm sputtered

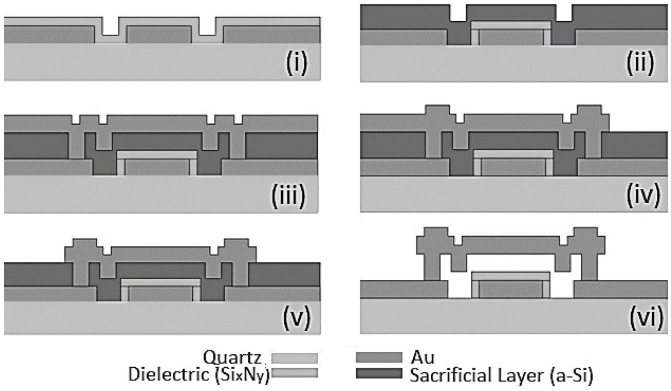

Fig. 12. Fabrication process for RF MEMS switch. i. Ti/Au CPW metal coating/etching and SixNy dielectric deposition. ii. SixNy dielectric etching and a-Si sacrificial layer deposition. iii. a-Si sacrificial layer anchor area opening and structural layer deposition. iv. Structural layer patterning and electroplating. v. Structural layer etching. vi. Releasing the MEMS bridge.

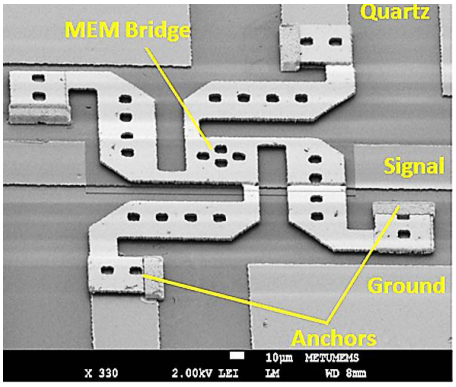

Fig. 13. SEM image of the suspended RF MEMS switch.

Au and Ti was used as an adhesion layer. The anchor areas were electroplated to strengthen these areas. The seed layer was etched after electroplating step. The fabrication steps are shown in Figure 12 and are listed below.

i. Ti/Au CPW metal coating/etching and Si_xN_y dielectric deposition.
ii. Si_xN_y dielectric etching and a-Si sacrificial layer deposition
iii. a-Si sacrificial layer anchor area opening and structural layer deposition
iv. Structural layer patterning and electroplating.
v. Structural layer etching
vi. Releasing the MEMS bridge

The MEMS bridge release process was done after seed layer etching step. The a-Si sacrificial layer etching was done by using XeF_2 etch system.

Figure 13 shows the released RF MEMS switch structure. As it can be seen, the MEMS bridge has four anchor, but just two of them are electrically connected to the ground. The other two anchors were formed on quartz wafer for mechanical support. This mechanical design simplifies the RF design, as well.

The deflection on the MEMS bridge was measured before and after thermal treatment. The measurements were taken at 20 °C, and then the switch was heated up to 200 °C in an oven. After 30 min. thermal treatment the temperature

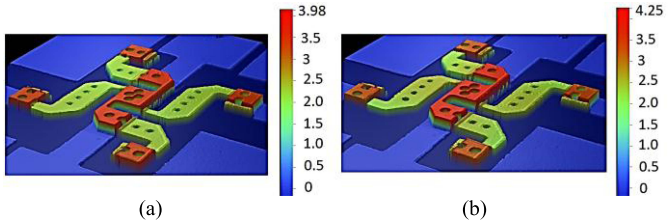

(a) (b)

Fig. 14. The fabricated RF MEMS switch surface profiler measurements. (a) at 20 °C after fabrication, (b) at 20 °C after 270 °C thermal treatment.

TABLE V
MEMS BRIDGE DEFLECTION FOR DIFFERENT TEMPERATURES

Thermal Treatment (°C)	Deflection (μm)	Δz (μm) Measurement	Δz (μm) Simulation
20	3.98	0	0
200	4.03	0.05	0.15
250	4.18	0.2	0.22
270	4.25	0.27	0.26

was decreased to 20 °C to repeat the measurements and no change was observed on the MEMS bridge buckling up to 200 °C. The measurements were taken for 250 °C and 270 °C thermal treatment and the permanent deformation was observed at these temperatures. Figure 14 shows the surface profiler measurement results for 20 °C and 270 °C thermal treatment. The deflection (Δz) on the middle part (on signal line) of the MEMS bridge was measured as 0.2 μm and 0.27 μm after 250 °C and 270 °C thermal treatment.

The simulation and measurement results of bridge deflection with temperature are given in TABLE V. The measurements results are in agreement with simulation results. As it can be seen the bridge deflection is 0.15 μm at 200 °C according to model but 0.05 μm deflection is measured after heat treatment. It can be said that, the MEMS bridge is expanded with temperature and rotated on the z axis at 200 °C. When the temperature is decreased to 20 °C the MEMS bridge returns to its original position with minimum deformation. However, the bridge can not return to its original position after 250 °C thermal treatment due to plastic deformation on the bridge.

The RF measurements were done before and after 200 °C thermal treatment to understand the thermal effects on RF performance of the switch. The switch actuation voltage and RF measurements were carried out after fabrication and then the switch was placed into the oven and the temperature was increased up to 200 °C. After 30 minutes of thermal treatment the actuation voltage and RF measurements were recorded again. Figure 15(a) shows the upstate S_{11} parameters of the switch. As it can be seen, there is no significant fluctuation in S-parameters and $S_{11} < -15$ dB up to 40 GHz, before and after 200 °C thermal treatment. The measured insertion loss is < 0.35 dB up to 40 GHz (Figure 15 (b)). The RF performance of the switch before and after thermal treatment was not effected. Therefore, the RF MEMS switch can be packaged at 200 °C. The isolation is another important parameter for desired frequency. The RF MEMS switch was design to get maximum isolation at 35 GHz but the measurement shows that the maximum isolation frequency is 33 GHz (37 dB). The dielectric layer was designed as 0.3 μm but in this fabrication

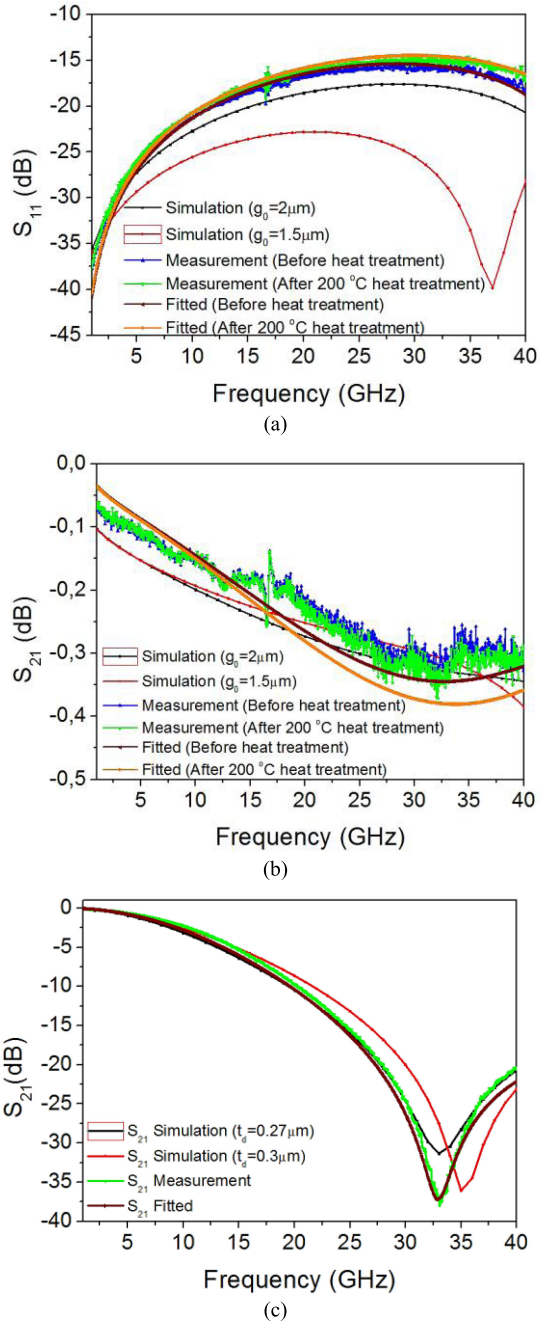

Fig. 15. S-parameters, simulation and measurement results, (a) Up state S_{11}, (b) up state S_{21} and, (c) down state S_{21} values of RF MEMS switch.

the thickness of this layer is 0.27 μm. It can be attributed to thinner Si_xN_y layer than designed value. Figure 15(c) shows the simulated and measured isolation of the RF MEMS switch for 0.3 and 0.27 μm-thick Si_xN_y. The isolation band for <-20 dB was measured as 28-40 GHz.

Fig.16 shows the equivalent circuit model of the RF MEMS switch. The switch capacitance at up/down state, inductance and resistance values were extracted by fitting the circuit model to the measured S-parameters. Up state capacitance values of the switch were extracted as 54 fF (C_u) and 51 fF (C_{u2}) before and after 200 °C thermal treatment, respectively. The downstate capacitance (C_d) is 0.6 pF at room temperature. The bridge inductance and resistance are found as 39 pH and 0.48 Ω from the model, respectively.

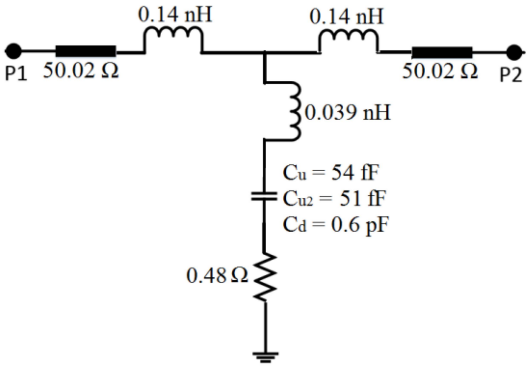

Fig. 16. Equivalent circuit model of RF MEMS switch.

IV. Conclusion

The temperature effect on the RF MEMS switch is an important issue. Especially, packaging temperature can damage MEMS bridge structure and result in permanent deformation on the bridge.

In this study, a new bridge geometry was designed to reduce the thermal expansion based permanent deformation on the MEMS bridge. This bridge has four fixed anchor and laterally movable mechanical arms under high temperature. The measurement results show that this lateral moving of the mechanical arms reduces the thermal expansion based stress level and permanent deformation on the MEMS bridge.

According to measurement results the electromechanical and RF performance fabricated RF MEMS switch are not changed after 200 °C thermal treatment. The switch shows permanent deformation with $\Delta z = 0.2$ and 0.27 μm at 250 °C and 270 °C respectively. The insertion loss and isolation are measured as < 0.3 dB and < 20 dB at 28-40 GHz band and in a good agreement with the simulation results. The actuation voltage is relatively low and measured as 22 V and 25 V before and after thermal treatment, respectively. The measured RF performance is compatible with the simulation result for 2 μm gap. According to the simulation results, the RF MEMS switch shows very low loss for 1.5 μm gap. In the future work, the switch will be fabricated with 1.5 μm air gap. This reduced gap will decrease the actuation voltage, as well.

Acknowledgement

The authors would like to thank ÇağrıÇetintepe for his support in the measurements.

References

[1] H. A. C. Tilmans, W. De Raedt, and E. Beyne, "MEMS for wireless communications: 'From RF-MEMS components to RF-MEMS-SiP,'" *J. Micromech. Microeng.*, vol. 13, no. 4, p. S139, Jun. 2003.

[2] D. Bansal, A. Kumar, A. Sharma, P. Kumar, and K. J. Rangra, "Design of novel compact anti-stiction and low insertion loss RF MEMS switch," *Microsyst. Technol.*, vol. 20, no. 2, pp. 337–340, May 2013.

[3] H.-H. Yang, A. Yahiaoui, H. Zareie, P. Blondy, and G. M. Rebeiz, "A compact high-isolation DC-50 GHz SP4T RF MEMS switch," in *Proc. IEEE MTT-S Int. Microw. Symp. (IMS)*, Jun. 2014, pp. 1–4.

[4] Y. Zhu and H. D. Espinosa, "Effect of temperature on capacitive RF MEMS switch performance—A coupled-field analysis," *J. Micromech. Microeng.*, vol. 14, no. 8, p. 1270, Jun. 2004.

[5] A. Somà and M. M. Saleem, "Modeling and experimental verification of thermally induced residual stress in RF-MEMS," *J. Micromech. Microeng.*, vol. 25, no. 5, p. 055007, Apr. 2015.

[6] L. L. Mercado, S.-M. Kuo, T.-Y. Lee, and R. Lee, "Analysis of RF MEMS switch packaging process for yield improvement," *IEEE Trans. Adv. Packag.*, vol. 28, no. 1, pp. 134–141, Feb. 2005.

[7] C. Zhao, J. Song, L. Han, and Q.-A. Huang, "Effects of thermally induced packaging stress on a distributed RF MEMS phase shifter," *Microsyst. Technol.*, vol. 21, no. 4, pp. 869–874, May 2014.

[8] C. L. Goldsmith and D. I. Forehand, "Temperature variation of actuation voltage in capacitive MEMS switches," *IEEE Microw. Wireless Compon. Lett.*, vol. 15, no. 10, pp. 718–720, Oct. 2005.

[9] V. Mulloni, G. Sordo, and B. Margesin, "Thermal cycling reliability of RF-MEMS switches," *Proc. SPIE*, vol. 9517, pp. 95170Q-1–95170Q-6, May 2015.

[10] C. Palego *et al.*, "Robustness of RF MEMS capacitive switches with molybdenum membranes," *IEEE Trans. Microw. Theory Techn.*, vol. 57, no. 12, pp. 3262–3269, Dec. 2009.

[11] R. Mahameed and G. M. Rebeiz, "RF MEMS capacitive switches for wide temperature range applications using a standard thin-film process," *IEEE Trans. Microw. Theory Techn.*, vol. 59, no. 7, pp. 1746–1752, Jul. 2011.

[12] I. Reines, B. Pillans, and G. M. Rebeiz, "Thin-film aluminum RF MEMS switched capacitors with stress tolerance and temperature stability," *J. Microelectromech. Syst.*, vol. 20, no. 1, pp. 193–203, Feb. 2011.

[13] R. Mahameed and G. M. Rebeiz, "A high-power temperature-stable electrostatic RF MEMS capacitive switch based on a thermal buckle-beam design," *J. Microelectromech. Syst.*, vol. 19, no. 4, pp. 816–826, Aug. 2010.

[14] Y. Shim, Z. Wu, and M. Rais-Zadeh, "A high-performance, temperature-stable, continuously tuned MEMS capacitor," in *Proc. IEEE 24th Int. Conf. Micro Electro Mech. Syst. (MEMS)*, Jan. 2011, pp. 752–755.

[15] R. M. Pocratsky and M. P. de Boer, "Determination of thin film coefficient of thermal expansion and residual strain from freestanding fixed–fixed beams," *J. Vac. Sci. Technol. B*, vol. 32, no. 6, p. 062001, Nov. 2014.

[16] G. M. Rebeiz, "Mechanical modeling of MEMS devices: Static analysis," in *RF MEMS: Theory, Design, and Technology*. Hoboken, NJ, USA: Wiley, 2004.

Kaan Demirel received the B.S. degree in physics engineering from Ankara University, in 2006. He is currently pursuing the Ph.D. degree in nanotechnology and nanomedicine from Hacettepe University. He was a Teaching Assistant with the Faculty of Engineering and Natural Sciences, Sabanci University, Istanbul, from 2007 to 2008. He was a Research Engineer with the Advanced Research Laboratory, Nanotechnology Research Center, Bilkent University, Ankara, from 2008 to 2009. He has been a Member of the RF MEMS Group with Middle East Technical University, since 2009. His research interests include RF MEMS switch design, process development, and microvacuum devices.

Erdem Yazgan received the B.S. and M.S. degrees from Middle East Technical University, Ankara, Turkey, in 1971 and 1973, respectively, and the Ph.D. degree from Hacettepe University, Ankara, in 1980, all in electrical and electronics engineering. In 1989, she was a Visiting Professor with Essex University, Essex, U.K. From 1994 to 1995, she was with the Electroscience Laboratory, Ohio State University, Columbus, USA. From 1990 to 2015, she was a Professor with the Department of Electrical and Electronics Engineering, Hacettepe University. She was an Advisor on the World Bank Industrial Training Project, TAFICS–NATO, TUBİTAK–Space Institude for Göktürk-II, METU, and the Information Technology Division Laboratory, H.U. Teknokent Radio–TV Standardization Committee of the Standardization Institute of Turkey and Defense Electronics Firms. She joined the Engineering Faculty, TED University, in 2015, as the Chair of Electrical-Electronics Engineering. Her research interests include HF Propagation, low-altitude radar systems, mobile communications, MIC's, reflector and microstrip antennas, gaussian beam solutions, conformal mapping, satellite communication, and medical electronics.

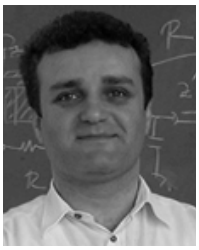

Şimşek Demir (S'91–M'98) received the B.Sc., M.Sc., and Ph.D. degrees in electrical and electronics engineering from Middle East Technical University (METU), Ankara, Turkey, in 1991, 1993, and 1998, respectively. From 1991 to 1998, he was a Research Assistant with METU. From 1998 to 1999, he contributed to the atmospheric radar antenna design with the International Research Centre for Telecommunications and Radar, Delft University of Technology, The Netherlands. Since 2000, he has been a Professor with the Electrical and Electronics Engineering Department, METU. His current research interests include microwave and millimeter-wave active and passive component, and system design, analysis, and modeling. His research topics include the exploitation of RF MEMS technology toward industrial use, power amplifier design and modeling, and has received several awards, including the NATO A2 Fellowship, which supported him as a Visiting Researcher with the University of Massachusetts, Amherst, in 1995.

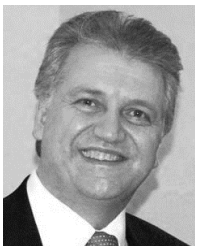

Tayfun Akın was born in Van, Turkey, in 1966. He received the B.S. (Hons.) degree from Middle East Technical University (METU), Ankara, in 1987, and the M.S. and Ph.D. degrees from the University of Michigan, Ann Arbor, in 1989 and 1994, respectively, all in electrical engineering. He went to USA in 1987 for his graduate studies with a graduate fellowship provided by the NATO Science Scholarship Program through the Scientific and Technical Research Council of Turkey. Since 1995, 1998, and 2004, he has been an Assistant Professor, an Associate Professor, and a Professor, respectively, with the Department of Electrical and Electronics Engineering, METU. He is currently the Director of the METU–Microelectromechanical Systems (MEMS) Center. He raised and managed over U.S. $65 million in funding for several national and international projects, including EU FP6, FP7, NATO SfS, and NSF–USA Projects. His current research interests include MEMS, microsystems technologies, uncooled infrared detectors and readout circuits, inertial microsensors, silicon-based integrated sensors and transducers, and analog and digital integrated circuit design. He was a recipient of the First Prize in Experienced Analog/Digital Mixed-Signal Design Category at the 1994 Student VLSI Circuit Design Contest organized and sponsored by Mentor Graphics, Texas Instruments, Hewlett-Packard, Sun Microsystems, and Electronic Design Magazine. He has co-authored the Symmetric and Decoupled Gyroscope project, which received the First Prize Award in the operational designs category of the International Design Contest organized by the DATE Conference and CMP in 2001. He has also co-authored the Gyroscope project, which received the Third Prize Award of the 3-D MEMS Design Challenge organized by MEMGen Corporation (currently, Microfabrica). He has served various MEMS, EUROSENSORS, and TRANSDUCERS Conferences, as a Technical Program Committee Member. He was the Co-Chair of the 19th IEEE International Conference of MEMS 2006, held in Istanbul, and he was the Co-Chair of the Steering Committee of the IEEE MEMS Conference in 2007. He is the Steering Committee Member of the 18th International Conference on Solid-State Sensors, Actuators, and Microsystems (Transducers 2015).